STATISTICS, OPTIMIZATION AND INFORMATION COMPUTING
*Stat., Optim. Inf. Comput.*, Vol. **15**, February 2026, pp 955–974.
Published online in International Academic Press (www.IAPress.org)

# Discrete Orthogonal Moment Descriptors Applied In Image Classification And Object Recognition Enhanced By Machine Learning Methods

Abdelati Bourzik [1,*], Belaid Bouikhalene [1], Jaouad El-Mekkaoui [2], Amal Hjouji [3]

[1] *LIMATI Laboratory, Polydisciplinary Faculty, Sultan Moulay Slimane University, Beni Mellal, Morocco*
[2] *LSEM Laboratory, Higher School of Technology, Sidi Mohamed Ben Abdellah University, Fez, Morocco*
[3] *STIC Laboratory, Faculty of Science, Sidi Mohamed Ben Abdellah University, Fez, Morocco*

**Abstract** Orthogonal moments play a crucial role in image analysis, including applications in image reconstruction and the extraction of consistent, robust features, making them essential for modern computational imaging. This study examines the effectiveness and performance evaluation of orthogonal: Tchebichef moments, Krawtchouk moments, Charlier moments, and Hahn moments for image reconstruction, feature description, and their application in image classification and object recognition using advanced machine learning techniques. We present the construction process of orthogonal image moments. Then the deriving of invariant moments based on Tchebichef, Krawtchouk, Charlier, and Hahn polynomials. These moments are then employed to generate feature vectors specifically tailored for image classification and object recognition tasks. To evaluate feature robustness, we conduct extensive classification experiments on two distinct image databases using K-Nearest Neighbors (K-NN) and Support Vector Machine (SVM) classifiers. The results demonstrate that invariant moments are highly effective at capturing discriminative image features and maintain reliable performance under various noise conditions, including salt-and-pepper noise, underscoring their applicability in real-world scenarios.

**Keywords** Image reconstruction, Orthogonal moments, Invariant Moments, Image Classification, Machine Learning.

**DOI:** 10.19139/soic-2310-5070-2538

## 1. Introduction

Discrete orthogonal moments are sets of mathematical functions that are especially helpful for identifying important aspects of a signal or image [1]. While, Invariant orthogonal moments are sets of mathematical functions that are invariant to geometric transformations such as rotation, translation, and scale changing. However, in the last decades, they have been useful for capturing significant features of an image or a signal [2, 1].

Image or signal moments are mathematical quantities that give a means of characterizing the distribution of samples or pixel intensities in a digital image or signal. used for the first time by Hu et al. [3]. But the moments of Hu are not orthogonal, which means that they can be easily affected by noise and redundancy. Whatever the moments of Hu are invariant to translation, scaling, and rotation, the drawback is that they are not orthogonal. Then, Teague et al. introduced in [4] the theory of orthogonal moments, where the image's projection on the orthogonal polynomial base's elements is used to compute the moments. They have been used a lot in jobs involving image recognition and analysis.

Numerous orthogonal moment types have been identified in the literature based on multiple polynomial bases. These moments have been classified as discrete and continuous, with examples for ones such as; Krawtchouk

---

[*] Correspondence to: Abdelati Bourzik (Email: abdelati.bourzik@usms.ac.ma). Department of Mathematics and computer science, Polydisciplinary Faculty, Sultan Moulay Slimane University, Beni Mellal, Morocco.

ISSN 2310-5070 (online) ISSN 2311-004X (print)
Copyright © 2026 International Academic Press

moments [5], Tchebichef moments [6, 7], Charlier moments [8, 9], Hahn moments [10, 11], Gegenbauer moments [12, 13], and Meixner moments [14]. And Legendre moments [15], Gegenbauer moments [12], Zernike moments [16], and Jacobi moments [17, 18] for continuous moments. All of these moments have been specified on a uniform lattice. On a non-uniform lattice however, other discrete moments, such as Dual Hahn moments [19] and Racah [20], are orthogonal. In our daily lives, there are various applications of orthogonal moments in certain fields, such as computer vision in autonomous cars [21], medical image analysis [22, 23], or facial recognition [24], object detection and recognition [25, 26].

In this paper, we compare some existing methods for image reconstruction and image classification, by the construction of invariant moments. These invariant moments computed for a given image and placed into a vector are considered a set of features. For instance, in first stage: we compared the image reconstruction by Tchebichef moments, Krawtchouk moments, Charlier moments, and Hahn moments, which are based respectively on orthogonal Tchebichef polynomials, orthogonal Krawtchouk polynomials, orthogonal Charlier polynomials, and orthogonal Hahn polynomials, with performance evaluation using mean square reconstruction error and peak signal to . In second stage: we studied the invariant version of studied moments and there performances in classification and recognition tasks, it is important that the method for deriving invariants is to formulate the given orthogonal moments as a function of geometric ones. The next step involves fitting the descriptor vector to a machine learning algorithm, which then trains the classification algorithm. The models used are K-Nearest Neighbors (K-NN) and Support Vector Machines (SVM). The methods are tested and evaluated in two different databases, as well as in the presence of salt and pepper noise.

This paper is organized as follows: Section 2 outlines a background about the studied discrete orthogonal polynomials. After that, section 3 shows the way for construction of image moments. This is followed in Section 4 by the formulation of invariant moments derived from geometric moments, focusing on four studied moments types: Tchebichef, Krawtchouk, Charlier, and Hahn. Section 5 presents results of image reconstruction and classification experiments to assess performance, followed by comparisons and discussions. Finally, the paper concludes with a summary.

## 2. Discrete Orthogonal Polynomials

In this section, we provide background on several well-known discrete orthogonal polynomials widely used in the field of image analysis through moments. These polynomials form the foundation for various techniques in image moment computation and analysis. Figure 1 Visualizes the plots of basis discrete polynomials up to order $4$.

### *2.1. Tchebichef polynomials*

The Tchebichef polynomials of order $n$ and discrete variable $x$ are given by using hypergeometric function as in table 3. Where, $x = 1, 2, \dots, N$ and ${}_3F_2(.)$ is the hypergeometric function defined by the following relation:

$${}_3F_2(a_1, a_2, a_3; b_1, b_2; x) = \sum_{k=0}^{+\infty} \frac{(a_1)_k (a_2)_k (a_3)_k}{(b_1)_k (b_2)_k} \frac{x^k}{k!} \tag{1}$$

with, $(a)_k$ is the ascending factorial symbol known as the Pochhammer symbol defined by [27]:

$$(a)_k = a(a+1)(a+2)\dots(a+k-1) \tag{2}$$

The polynomials $t_p(x)$ have the following recurrence relation, concerning the variable $x$ [28]:

$$t_p(x) = \alpha_p(x) t_p(x-1) + \beta_p(x) t_p(x-2),\ x = 2, 3, \dots, \frac{N}{2} \tag{3}$$

Where $p = 1, 2, \dots N$, and $\alpha$ and $\beta$ are two functions given as:

$$\alpha_p(x) = \frac{-p(p+1) - (2x-1)(x-N-1) - x}{x(N-x)} \tag{4}$$

$$\beta_p(x) = \frac{(x-1)(x-N-1)}{x(N-x)} \tag{5}$$

The following equations can be used to get the moments in $x = 0$ and $x = 2$ for the initialization of the recursion equation (3) [28].

$$t_p(0) = -\sqrt{\frac{N-p}{n+p}}\sqrt{\frac{2p+1}{2p-1}}t_{p-1}(0) \tag{6}$$

$$t_p(1) = t_p(0)\left(1 + \frac{p(1+P)}{1-N}\right) \tag{7}$$

To reduce the algorithm complexity at the moment calculation level or at the reconstruction level, the symmetry property of orthogonal moments can be applied by [28]:

$$t_p(N-1-x) = (-1)^p t_p(x) \tag{8}$$

### *2.2. Krawtchouk polynomials*

The definition of Krawtchouk polynomials for the $n-th$ order is defined as in table 3. Where $x, n = 1, 2, \dots, N$, $0 \leqslant p \leqslant 1$ and ${}_3F_1$is the hypergeometric function, defined as:

$${}_3F_1(a; b; c, x) = \sum_{k=0}^{+\infty} \frac{(a)_k (b)_k}{((c)_k} \frac{x^k}{k!} \tag{9}$$

and with $(a)_k$ is the Pochhammer symbol defined before, and the functions with weight function for the Krawtchouk polynomials is given in table 2. The recurrence relation in three terms for the normalized and weighted Krawtchouk polynomials is as follows [29]:

$$p(n-N)\widehat{k}_{n+1}^{(p,N)}(x) = A_n[p(N-2n) - x + n]]\widehat{k}_n^{(p,N)}(x) - B_n(1-p)\widehat{k}_{n-1}^{(p,N)}(x) \tag{10}$$

Where,

$$A_n = \sqrt{\frac{(1-p)(n+1)}{(p(N-n)}}; \quad B_n = \sqrt{\frac{(1-p)^2(n+1)n}{(p^2(N-n)(N-n+1)}} \tag{11}$$

Such that, the initialization values of recurrence relation (10) as in [29] are:

$$\widehat{k}_0^{(p,N)}(x) = \sqrt{\omega_k(p, N, x)}; \quad \widehat{k}_1^{(p,N)}(x) = \left(1 - \frac{1}{p \times N}x\right)\sqrt{\omega_k(p, N, x)} \tag{12}$$

### *2.3. Charlier polynomials*

On the other hand, Charlier polynomials are defined up to the $n$th order according to Zhu et al. [30] by the following equation in table 3. The generalized hyper-geometric function ${}_2F_0$ is defined as follows: $n$ is the order of polynomials; $a_1$ is the Charlier polynomial parameter, which is a positive real number.

$${}_2F_0(a; b, x) = \sum_{k=0}^{+\infty} (a)_k (b)_k \frac{x^k}{k!} \tag{13}$$

The Pochhammer symbol, $(a)_k$, was originally provided previously in 2.

Charlier's discrete orthogonal polynomials satisfy the following three-term recurrence relation with respect to $n$

[31]:

$$\widehat{c}_{n+1}^{(a_1)}(x) = \frac{a_1 - x + n + 1}{a_1}\sqrt{\frac{a_1}{n}}\widehat{c}_n^{(a_1)}(x) - \sqrt{\frac{n-1}{n}}\widehat{c}_{n-1}^{(a_1)}(x) \tag{14}$$

The initialization values are as follows [31]:

$$\widehat{c}_0^{(a_1)}(x) = \sqrt{\frac{\omega_c(a_1, x)}{\sigma_c(a_1, 0)^2}}; \quad \widehat{c}_1^{(a_1)}(x) = \frac{a_1 - x}{a_1}\sqrt{\frac{\omega_c(a_1, x)}{\sigma_c(a_1, 1)^2}} \tag{15}$$

### *2.4. Hahn polynomials*

The Hahn polynomials of order $n$, are defined on a nonuniform lattice according to [11, 32] by the following equation in table 3. Where $x, n = 1, 2, \ldots, N$ is the order of moments and $\alpha, \beta$ are positive integers. and ${}_3F_2$is the known generalized hyper-geometric function, defined as:

$${}_3F_2(a, b, c; d, e; x) = \sum_{k=0}^{+\infty} \frac{(a)_k(b)_k((c)_k}{(e)_k(d)_k}\frac{x^k}{k!} \tag{16}$$

Therefore to achieve numerical stability, a set of weighted Hahn polynomials are introduced in [5]:

$$\widehat{H}_n^{(\alpha,\beta,N)}(x) = H_n^{(\alpha,\beta,N)}(x)\sqrt{\frac{\omega_h(\alpha, \beta, N, x)}{\sigma_h(\alpha, \beta, N, n)}} \tag{17}$$

Where, $\omega_h(\alpha, \beta, N, x)$ and $\sigma_h(\alpha, \beta, N, n)$ are the weight and squared norm functions defined in table 2.
The three term recurrence relation in the n-direction for the normalized and weighted Hahn polynomials is given as follows [30]:

$$\widehat{H}_n^{(\alpha,\beta,N)}(x) = \frac{AB}{E}\widehat{H}_{n-1}^{(\alpha,\beta,N)}(x) + \frac{CD}{E}\widehat{H}_{n-2}^{(\alpha,\beta,N)}(x) \tag{18}$$

Where the parameters A, B, C , D and E are given in table 1. And the initialization of recurrence relation in 32 is as follows [30]:

$$\widehat{H}_0^{(\alpha,\beta,N)}(x) = \sqrt{\frac{\omega_h(\alpha, \beta, N, x)}{\sigma_h(\alpha, \beta, N, 0)}} \tag{19}$$

$$\widehat{H}_1^{(\alpha,\beta,N)}(x) = (x(\alpha + \beta + 2) - (\beta + 1)(N - 1)) \times \sqrt{\frac{\omega_h(\alpha, \beta, N, x)}{\sigma_h(\alpha, \beta, N, 1)}} \tag{20}$$

## 3. Construction of Image Moments

This section outlines the process of computing image moments. We construct orthogonal moments for three types of images: binary, grayscale, and color, detailing the unique considerations and methods used for each image type.

### *3.1. For binary and grayscale images*

Consider a $M \times N$ rectangular grid of pixels with M-rows and N-columns that represents the image $f(x, y)$. To keep things simple, we use a picture with an equal number of rows and columns that is $N \times N$ in size. However, for a given image of size $N \times N$, with values in the range $[0, N - 1]$ for $x$ and $y$, let $N$ be a positive integer. The following formula is used to define the orthogonal image moments noted OMs:

$$OM_{nm} = \sum_{x=0}^{N-1}\sum_{y=0}^{N-1} OP_n(x)OP_m(y)f(x, y) \tag{21}$$

Table 1. Data for descret Hahn polynomials

$$
\begin{array}{lcl}
\text{A} & = & x - \dfrac{\alpha-\beta+2N-2}{4} - \dfrac{(\beta^2-\alpha^2)(\alpha+\beta+2N)}{4(\alpha+\beta+2n-2)(\alpha+\beta+2n)} \\
\text{B} & = & \sqrt{\dfrac{n(\alpha+\beta+n)(\alpha+\beta+2n+1)}{(N-n)(\alpha+n)(\beta+n)(\alpha+\beta+2n-1)(\alpha+\beta+N+n)}} \\
\text{C} & = & -\dfrac{(\alpha+n-1)(\beta+n-1)(\alpha+\beta+N+n-1)(N-n+1))}{(\alpha+\beta+2n-2)(\alpha+\beta+2n-1)} \\
\text{D} & = & \sqrt{\dfrac{n(n-1)(\alpha+\beta+n)(\alpha+\beta+n-1)(\alpha+\beta+2n-1)}{(\alpha+n)(\beta+n)(\alpha+n-1)(\beta+n-1)(N-n+1)(N-n)}} \\
 & & \times\sqrt{\dfrac{1}{(\alpha+\beta+2n-3)(\alpha+\beta+N+n)(\alpha+\beta+N+n-1)}} \\
\text{E} & = & \dfrac{n(\alpha+\beta+n)}{(\alpha+\beta+2n-1)(\alpha+\beta+2n)}
\end{array}
$$

Table 2. Data for some discrete orthogonal polynomials.

| Polynomial | Symbol | Weight function | Squared norm function |
|---|---|---|---|
| Tchebichef [28] | $t_n(x)$ | $\omega_t = 1$ | $\sigma_t(n,N) = \sum_{n=1}^{N}\{t_n(x)\}^2 = \frac{N(1-\frac{1^2}{N^2})(1-\frac{2^2}{N^2})\dots 1-\frac{n^2}{N^2})}{2n+1}$ |
| Krawtchouk [5] | $k_n^{(p)}(x)$ | $\omega_k(p,N,x) = \binom{x}{N} p^x(1-p)^{N-x}$ | $\sigma_k(p,N,n) = \left(\frac{p-1}{p}\right)^n \frac{n!}{(-N)_n}$ |
| Charlier [8] | $c_n^{(a_1)}(x)$ | $\omega_c(a_1,x) = \frac{e^{-a_1}a_1^x}{x!}$ | $\sigma_c(a_1,n) = \frac{n!}{a_1^n}$ |
| Hahn [11] | $h_n^{(\alpha,\beta)}(x)$ | $\omega_h(\alpha,\beta,N,x) = \frac{\Gamma(\beta+1+x)\Gamma(N-x+\alpha)}{\Gamma(x+1)\Gamma(N-x)}$ | $\sigma_h(\alpha,\beta,N,n) = \frac{(\alpha+\beta+n+1)_N\Gamma(\beta+1+n)\Gamma(\alpha+1+n)}{(2n+\alpha+\beta+1)\Gamma(n+1)\Gamma(N-n)}$ |

Table 3. Hypergeometric form for some discrete orthogonal polynomials.

| Polynomial | | Hyper-geometric function |
|---|---|---|
| Tchebichef [28] | $t_p(x) =$ | $(1-N)_{n\,3}F_2(-n-x, 1+n; 1, 1-N; 1)$ |
| Krawtchouk [5] | $k_n^{(p,N)}(x) =$ | ${}_2F_1(-n, -x; -N; \frac{1}{p})$ |
| Charlier [30] | $c_n^{(a_1)}(x) =$ | ${}_2F_0(-n, -x; ; \frac{-1}{a_1})$ |
| Hahn [11] | $h_n^{(\alpha,\beta,N)}(x) =$ | ${}_3F_2(-n, n+\alpha+\beta+1, -x; \alpha+1, -N; 1)$ |

Where, OP represent orthogonal polynomials such as Tchebichef, Krawtchouk, Charlier, Hahn. It is important to observe that these polynomials are orthogonal in order to eliminate redundancy and less sensitive to noise. However, they verify the following orthogonality condition:

$$\sum_{x=1}^{N-1} \omega_p(.) OP_n(x) OP_m(x) = \sigma_p(.)\delta_{nm} \tag{22}$$

Where, $\omega_p(.)$ is the weight function, and $\sigma_p(.)$ is the square norm function for the used polynomial basis, the table 2 represent the weight and squared norm functions for some orthogonal polynomials. And $\delta_{nm}$ is the Kronecker symbol given by:

$$\delta_{nm} = \begin{cases} 1 \;\; if \;\; n = m; \\ 0 \;\; elswhere \end{cases} ; \tag{23}$$

Whereas, in order to attain numerical stability, a set of weighted polynomials are introduced by as follow:

$$\widehat{OP}_n(x) = OP_n(x)\sqrt{\frac{\omega_p(.)}{\sigma_p(.)}} \tag{24}$$

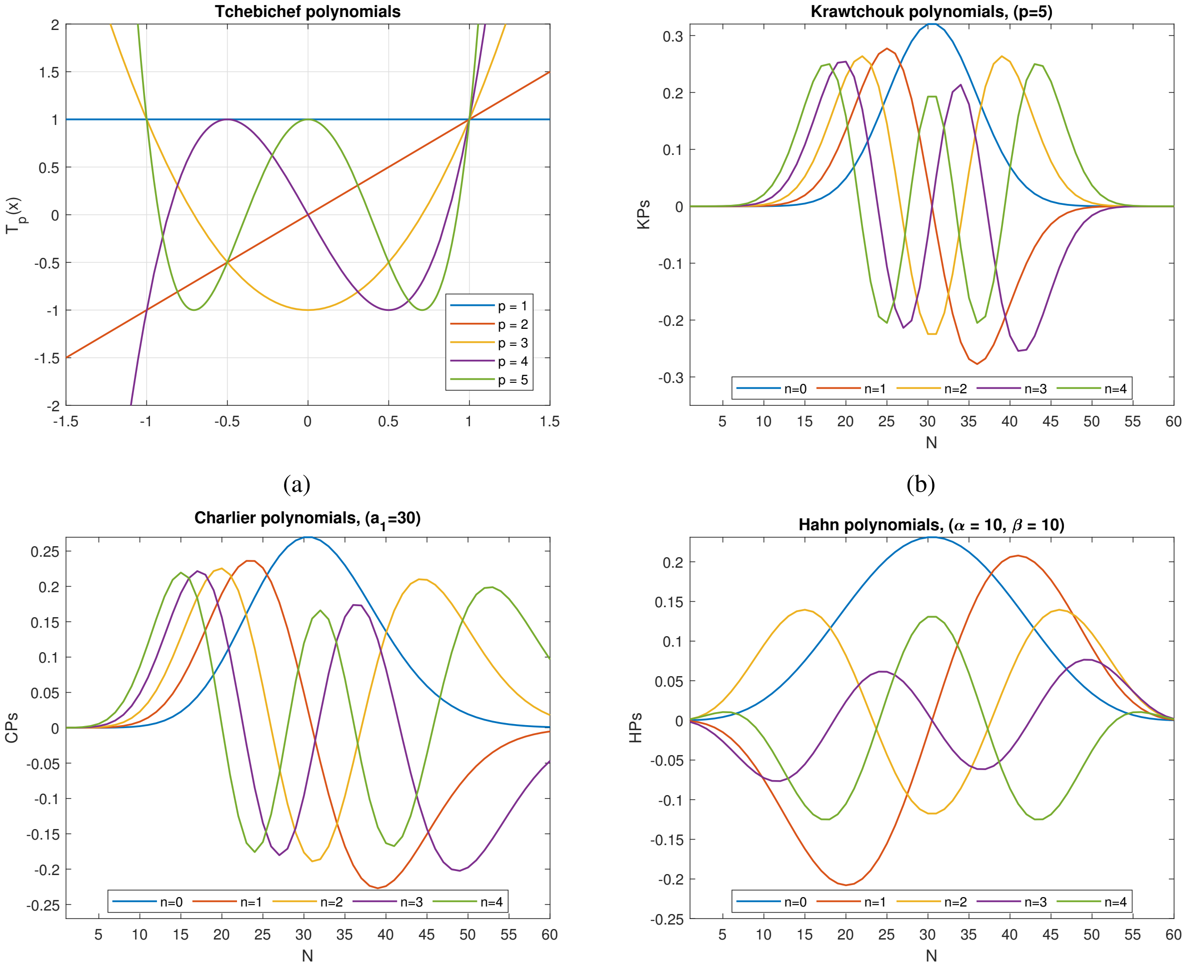

(a) (b)

(c) (d)

Figure 1. Discrete orthogonal polynomials as a function of 60 samples from order 0 to 4.

Consequently, using just the moment up to $n_{max}$, the reconstructed image $\widehat{f}(x, y)$ from OMs at a maximum order $n_{max}$ is obtained using the following relation [28]:

$$\widehat{f}(x, y) = \sum_{i=1}^{n_{max}-1} \sum_{j=1}^{n_{max}-1} OP_i(x) OM_{ij} OP_j(y) \tag{25}$$

### 3.2. *For color images*

For a color image $f_{color}(x, y)$ defined on three square channels $N \times N \times 3$. We compute the moments for each color channel of a color image [33]. Let a color image $f_{color}(x, y)$ be represented by the red (R), green (G), and blue (B), which are primary color channels, color image can be given as the following equation:

$$f_{color}(x, y) = \Big( f_R(x, y), f_G(x, y), f_B(x, y) \Big). \tag{26}$$

In the multi-channel OMs framework, OMs of each color component is computed. Hence, the set of OMs of color image is represented by:

$$OM_{nm}(f_{color}) = \Big(OM_R(f_R), OM_G(f_G), OM_B(f_B)\Big) \tag{27}$$

Next, given $k \in \{R, G, B\}$, the multi-channel orthogonal moments are defined as follows:

$$OM_{nm}(f_k) = \sum_{x=0}^{N-1}\sum_{y=0}^{N-1} OP_n^{(p,N)}(x) OP_m^{(a_1)}(y) f_k(x,y) \tag{28}$$

The color image is reconstructed using the following method if the value of the maximum order of moments, $n_{max}$, is the same for each component image:

$$\widehat{f}_k(x,y) = \sum_{i=1}^{n_{max}-1}\sum_{j=1}^{n_{max}-1} OP_i(x) OM_{ij}(f_k) OP_j(y) \tag{29}$$

The reconstructed color image $\widehat{f}_{color}(x,y)$ is the set of reconstructed color components of R, G, and B channels where:

$$\widehat{f}_{color}(x,y) = \Big(\widehat{f}_R(x,y), \widehat{f}_G(x,y), \widehat{f}_B(x,y)\Big). \tag{30}$$

### *3.3. Algorithm*

To decrease the complexity and enhance the speed of calculation time of 2-dimensional OMs of order $n$ for image $f$ we are using the matrix formulation in table 4.

Table 4. Matrix formulation for fast OMs computing

| Orthogonal Moments computation | Reconstructed image |
|---|---|
| $OM_{nm} = \widehat{OP}_n^T \times f \times \widehat{OP}_m$ | $\widehat{f} = \widehat{OP}_n \times OM_{nm} \times \widehat{OP}_m^T$ |

Where,

$$\begin{aligned} \widehat{OP}_n &= \Big[\widehat{OP}_0(x), \widehat{OP}_1(x), \ldots, \widehat{OP}_{n-1}(x)\Big] \\ \widehat{OP}_m &= \Big[\widehat{OP}_0(y), \widehat{OP}_1(y), \ldots, \widehat{OP}_{m-1}(y)\Big] \end{aligned} \tag{31}$$

denote the matrices of discrete $\widehat{OP}_n$ are orthogonal polynomials computed respectively up to the orders $n$ and $m$. In Algorithm 1, we provide a summary of the procedures involved in calculating orthogonal moments OMs, with respect to order $n$ for a given image $f(x,y)$.

**Algorithm 1** Computation of Orthogonal Moments (OMs)

```
Input: Input image $f(x,y)$ and desired moment order $n$.
Compute orthogonal polynomials (OPs) up to order $n$ using the recurrence relation.
Calculate Orthogonal Moments (OMs) for the input image using the matrix formulation provided in table 4.
Compute the $\widehat{f}(x,y)$ using the calculated OMs using the matrix formulation.
Determine the error MSE between $\widehat{f}(x,y)$ and $f(x,y)$.
Output: Reconstructed $\widehat{f}(x,y)$ image, Peak Signal-to-Noise Ratio (PSNR) and Mean Squared Error (MSE).
```

## 4. Invariability of Moments

In this section, we will show the very used technique to construct the invariant moments by making a relation with the known geometric ones.

### 4.1. *Invariant geometric moments*

For a digital image $f(x, y)$ with size $N \times N$, the geometric moments of order $n + m$ are defined using discrete sum approximation as:

$$GM_{nm} = \sum_{x=0}^{N-1} \sum_{y=0}^{N-1} x^n y^m f(x, y) \tag{32}$$

However, we can acquire translation invariants by moving the coordinate origin to the centroid of the image. Such that, $\mu_{nm}$ are the central geometric moments defined by Teague et al. in [4] by:

$$\mu_{nm} = \sum_{x=0}^{N-1} \sum_{y=0}^{N-1} (x - x_0)^n (y - y_0)^m f(x, y) \tag{33}$$

Where, $x_0 = \dfrac{m_{10}}{m_{00}}$, $y_0 = \dfrac{m_{10}}{m_{00}}$.

Then, the invariant to rotation are achieved by the conversion of the inertia principal axes system from the Cartesian coordinate system. The transformation relation is expressed as follows:

$$x' = xcos(\theta) + ysin(\theta), \quad y' = ycos(\theta) - xsin(\theta) \tag{34}$$

With, $\theta$ angle obtained by :

$$\theta = \frac{1}{2} tan^{-1} \left( \frac{2\mu_{11}}{\mu_{20} - \mu_{02}} \right) \tag{35}$$

The invariant to image translation and rotation is held using the following global equation.

$$\widehat{\mu}_{ij} = \sum_{x=0}^{N-1} \sum_{y=0}^{N-1} ((x - x_0)cos(\theta) + (y - y_0)sin(\theta))^i \times ((y - y_0)cos(\theta) - (x - x_0)sin(\theta))^j f(x, y) \tag{36}$$

Scale-invariant of $\mu_{ij}$ are accomplished by the normalization of each moment, where the normalized central geometric moment $GMI_{nm}$ of order $n + m$ is defined as:

$$GMI_{nm} = \frac{\widehat{\mu}_{nm}}{\widehat{\mu}_{nm}^{\gamma}} \tag{37}$$

Where the $\gamma = \dfrac{n + m + 2}{2}$.

Note that the set of invariant geometric moments GMIs by rotation, scaling and translation can be written as [3]:

$$GMI_{nm} = \frac{1}{(GM_{00})^{\gamma}} \sum_{x=0}^{N-1} \sum_{y=0}^{M-1} [(x - \overline{x})cos(\theta) + (y - \overline{y})sin(\theta)]^n \times [((y - \overline{y})cos(\theta) - (x - \overline{x})sin(\theta)]^m \tag{38}$$

With,

$$\overline{x} = \frac{MG_{10}}{MG_{00}}; \quad \overline{y} = \frac{MG_{01}}{MG_{00}} \tag{39}$$

And,

$$\gamma = \frac{n + m}{2} + 1; \quad \theta = \frac{1}{2} \frac{2\mu_{11}}{\mu_{20} - \mu_{02}} \tag{40}$$

Such that $\mu_{nm}$ are the central geometric moments defined by:

$$\mu_{nm} = \sum_{x=0}^{N-1} \sum_{y=0}^{M-1} (x-\overline{x})^n (y-\overline{y})^m f(x,y) \tag{41}$$

It is known that the relation between geometric moments and invariante ones is given by:

$$V_{nm} = \sum_{p=0}^{n} \sum_{q=0}^{m} (n,p)\,(m,q) \left(\frac{N \times M}{2}\right)^{\frac{p+q}{2}+1} \times \left(\frac{N}{2}\right)^{(n-p)} \times \left(\frac{M}{2}\right)^{(m-q)} \times GMI_{pq} \tag{42}$$

### *4.2. Invariant orthogonal moments*

There are numerous types of moments defined based on the choice of polynomial basis. In this study, we will explore specific examples of invariant orthogonal moments (OMIs) and their invariance to three primary geometric transformations: translation, rotation, and scaling by forming them as a function of invariant geometric moments GMIs.

*4.2.1. Tchebichef invariant moments* The Tchebichef polynomials can be expanded using power series [34] by the following relation:

$$\widehat{t}_n(x) = \sum_{k=0}^{p} C(p,k)(-x)_k \tag{43}$$

Where, $C(p,k)$ is a function given by:

$$C(p,k) = \frac{(-1)^p}{\sqrt{\sigma(p,N)}} \frac{(p+k)!}{(p-k)!(k!)^2} \frac{(N-K-1)!}{(N-p-1)!} \tag{44}$$

and $(x)_k$ are the Pochhammer symbol, that can be given as a function of first kind Stirling function as follow:

$$(x)_k = \sum_{i=0}^{k} (-1)^{k-i} s_1(k,i) x^i \tag{45}$$

Where, the first kind Stirling numbers are given by:

$$s_1(k,i) = s_1(k-1,i-1) - (k-1)s_1(k-1,i) \tag{46}$$

Where, $s_1(0,0) = 1$, $s_1(0,i) = 0$ and $s_1(k,0) = 0$. After some substituting equations the scaled Tchebichef polynomials are [34]:

$$\widehat{t}_p(x) = \sum_{k=0}^{p} \sum_{i=0}^{k} C(p,k)(-1)^{k-i} s_1(k,i) x^i = \sum_{i=0}^{p} B(i) x^i \tag{47}$$

And, $B(i) = \sum_{k=i}^{p} (-1)^k C(p,k) s_1(k,i)$.

In order to express the Tchebichef moments as a linear combination of geometric moments, the above equation is used so the TMs becomes:

$$TM_{nm} = \sum_{i=1}^{n} \sum_{j=1}^{m} B(i)B(j)GM_{ij} \tag{48}$$

Where, $GM_{nm}$ are the known geometric moments given before in the equation 32. The rotation, translation, and scaling invariants of Tchebichef moments can be formed using the correspondence with invariants of geometric moments [4].

Replacing geometric moments $GM_{ij}$ on the equation 48 with invariant geometric ones $\nu_{ij}$, the rotation, translation and scaling Tchebichef moments invariant's $TMI_{nm}$ are obtained according to [35] as the following:

$$TMI_{nm} = \sum_{i=0}^{n} \sum_{j=0}^{m} B(i)B(j)GMI_{ij} \tag{49}$$

*4.2.2. Krawtchouk invariant moments* The Krawtchouk polynomials can be written according to to Zhi et al. [36], by the following equation:

$$k_n^{(p,N)}(x) = \sum_{i=0}^{n} \alpha_{n,i}^{(p)} x^i \tag{50}$$

Where,

$$\alpha_{n,i}^{(p)} = \sum_{k=i}^{n} \frac{(-1)^k n!(N-k)!}{N!k!(n-k)!p^k} s(k,i) \tag{51}$$

For expressing Krawtchouk moments as in function of geometric ones the equation 50, is used to formulate Krawtchouk moments as follow citezhi2018translation:

$$KM_{nm} = \sum_{i=0}^{n} \sum_{j=0}^{m} \alpha_{n,i}^{(p)} \alpha_{m,j}^{(p)} GM_{ij} \tag{52}$$

Then, it can be easily derive the Krawtchouk moments invariant's (KMIs) from the geometric ones as follow;

$$KMI_{nm} = \sum_{x=0}^{n} \sum_{y=0}^{m} \alpha_{n,x}^{(p)} \alpha_{m,y}^{(p)} V_{nm} \tag{53}$$

*4.2.3. Charlier invariant moments* The same for charlier polynomials which can be obtained by [37]:

$$c_n(x) = \sum_{i=0}^{n} \beta_{n,i}^{(a_1)} x^i \tag{54}$$

Where,

$$\beta_{n,i} = \sum_{k=i}^{n} \frac{n!}{(n-k)!k!(n-k)!(-a_1)^k} s(k,i) \tag{55}$$

where, $s(k,i)$ are the Stirling numbers defined in 46. Then the CMs for an image $f(x,y)$ can be written as follow:

$$CM_{nm} = \sum_{x=0}^{N-1} \sum_{y=0}^{N-1} c_n(x) c_m(y) f(x,y) = \sum_{x=0}^{n} \sum_{y=0}^{m} \beta_{n,x} \beta_{m,y} GM_{x,y}(f) \tag{56}$$

then it can be easily derive the Charlier moments invariant's (CMIs) from the geometric ones as follow [37];

$$CMI_{nm} = \sum_{x=0}^{n} \sum_{y=0}^{m} \beta_{n,x} \beta_{m,y} V_{nm} \tag{57}$$

*4.2.4. Hahn invariant moments* According to [38] Hahn polynomials can be written also as the following:

$$h_n^{\alpha,\beta}(x) = A_n^\beta \sum_{k=0}^{n} B_{n,k}^{\alpha,\beta} < x >_k \tag{58}$$

Where,

$$A_n^\beta = \frac{(-1)^n(\beta+1)_n(N-n)_n}{n!} \tag{59}$$

and,

$$B_{n,k}^{\alpha,\beta} = \frac{(-n)_k(n+\alpha+\beta+1)_k}{(-1)^k k!(\beta+1)k(1-N)_k} \tag{60}$$

with, $< x >_k = \sum_{i=0}^{k} s(k,i)x^i$ the HPs becomes:

$$h_n^{\alpha,\beta}(x) = A_n^\beta \sum_{k=0}^{n} B_{n,k}^{\alpha,\beta} \sum_{i=0}^{k} s(k,i)x^i = \sum_{i=0}^{n} \phi_{n,i}^{\alpha,\beta} x^i \tag{61}$$

where, $\phi_{n,i}^{\alpha,\beta} = A_n^\beta \sum_{k=0}^{n-1} B_{n,n-k}^{\alpha,\beta} \sum_{i=0}^{k} s(n-k,i)$

Then the HMs for an image $f(x,y)$ can be written as follow:

$$HM_{nm} = \sum_{x=0}^{N-1}\sum_{y=0}^{N-1} h_n^{\alpha,\beta}(x)h_m^{\alpha,\beta}(y)f(x,y) = \sum_{x=0}^{n}\sum_{y=0}^{m} \phi_{n,x}^{\alpha,\beta}\phi_{m,y}^{\alpha,\beta} GM_{x,y}(f) \tag{62}$$

After that, it can be easily derive the Hahn moments invariant's (HMIs) orders up to $n+m$ from the geometric ones as follow;

$$HMI_{nm} = \sum_{x=0}^{n}\sum_{y=0}^{m} \phi_{n,x}^{\alpha,\beta}\phi_{m,y}^{\alpha,\beta} V_{nm} \tag{63}$$

$V_{nm}$ has a combination to invariant geometric moments in equation 42.

In Algorithm 2, the explanation of computation of orthogonal moments invariants OMIs based on making a relation between discrete moments and geometric ones.

**Algorithm 2** Computation of Orthogonal Moment's Invariants (OMIs)

```
Input: Input image $f(x,y)$ and desired moment order $n, m$.
1: Compute invariant geometric moments $GMI_{nm}$ for order $n, m$ using the equation 38.
2: Compute function $V_{nm}$ that makes relation between $GM_{nm}$ and $GMI_{nm}$ in equation 42.
3: Compute invariant moments for order $n, m$ using the formulation as geometric ones using 48,or 53, or 53,or
   53 depending on the type of invariant moments desired.
4: Do the same thing for all the orders required in vector 66.
Output: Vector that contains the OMIs features of image $f$.
```

## 5. Evaluation and Results

Discrete orthogonal moments OMs, have demonstrated significant practical utility across various real-world domains beyond synthetic datasets. In medical imaging, particularly in tumor detection using MRI and CT scans, OMs like Zernike moments have been used to extract rotation- and scale-invariant features that enhance

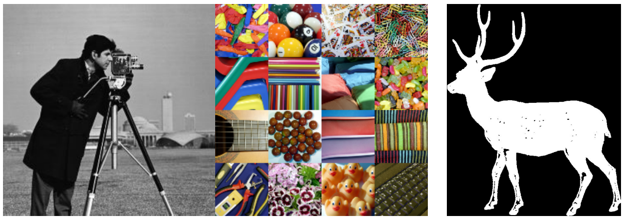
(a) (b) (c)

Figure 2. The test images : **(a)** Gray scale ”Cameraman” of size $500 \times 500$. **(b)**: Color ”Texture” image of size $1024 \times 1024$. **(c)**: Binary ”Deer” image of size $200 \times 200$.

tumor classification accuracy and aid in precise boundary delineation [39]. In the domain of autonomous driving, Tchebichef moments have been employed for robust road sign recognition under challenging conditions, leading to improved accuracy and faster inference in embedded systems [40]. These applications underscore the advantages of OMs, including their orthogonality, invariance to geometric transformations, computational efficiency, and interpretability, making them highly effective in practical, real-world scenarios. In this section, we apply these moments to image classification and object recognition.

The following results are divided into two parts to effectively evaluate the performance of the studied discrete orthogonal moments. The first part presents experimental results for reconstructing a given image, while the second part focuses on applying these moments in image classification and object recognition tasks using machine learning.

It is crucial to select the appropriate parameters for orthogonal moments based on parametric polynomials, such as Krawtchouk, Charlier, and Hahn polynomials. Specifically, for Krawtchouk polynomials, the parameter $p$ should be set to $0.5$, and for Charlier polynomials, the parameter $a_1$ should be set to $10$. These values are commonly used in the literature, and gives the best performance. We have a research on parameter optimization for Krawtchouk and Charlier is presented in [9]. For Hahn polynomials, setting both $\alpha = 10$ and $\beta = 10$ provides also the best performance, as demonstrated in [10].

### *5.1. Image reconstruction by OMs*

In order to prove the efficiency of orthogonal moments (OMs) for image analysis, the inverse procedure of construction of orthogonal moments can be done. Where the original image in figure 2 can be reconstructed using just the computed moments like given in equation 25. The evaluation is considered the mean square reconstruction error given in the following relation:

$$MSE = \frac{1}{N^2}\sum_{x=1}^{N}\sum_{y=1}^{N}\left(\widehat{f}(x,y) - f(x,y)\right)^2 \tag{64}$$

In the following we will consider three type of images: Binary, grayscal, and color images.

For color images, we will assume that the MSE is the mean of the MSEs along the three channels $R$, $G$, and $B$, where $MSE(f_{color}) = \frac{MSE(f_R)+MSE(f_G)+MSE(f_B)}{3}$. The reconstruction error for each channel is given as follows:

$$MSE(f_k) = \frac{1}{N^2}\sum_{x=1}^{N}\sum_{y=1}^{N}\left(\widehat{f_k}(x,y) - f_k(x,y)\right)^2 \tag{65}$$

Where, $k \in \{R, G, B\}$.

Figures 3 shows the compared TMs, KMs, CMs and HMs’s MSE as a function applied for binary, gray scale and color image. From the curves the MSE decrease while the order of moments as well. KMs are failed in some high orders. Where, TMs gives the best accuracy followed by HMs and CMs.

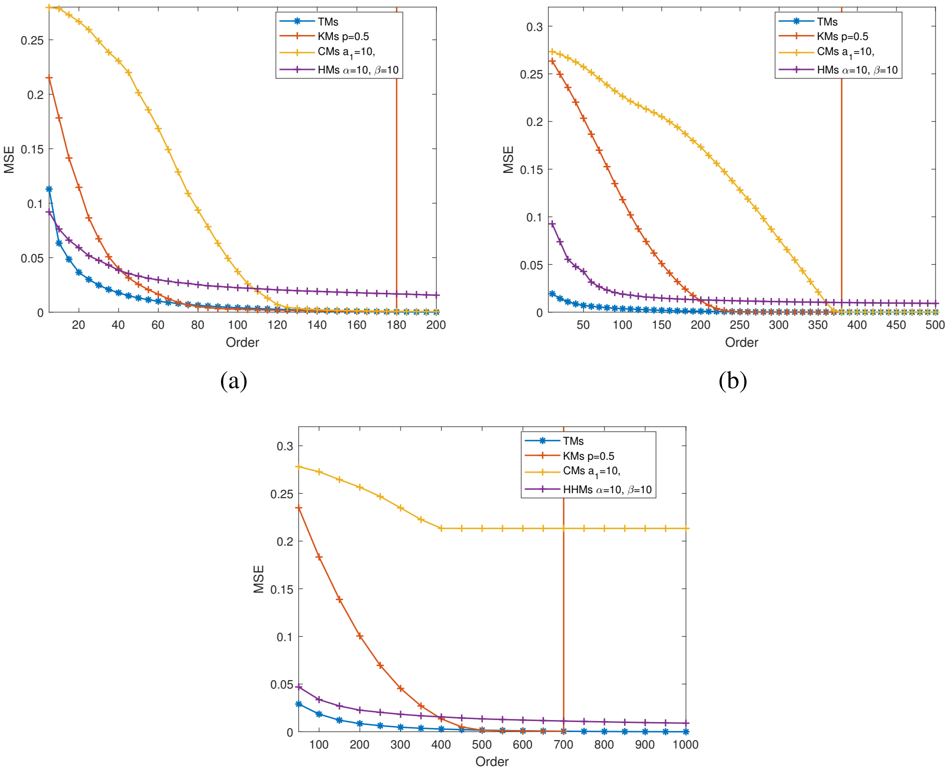

(a) (b)

(c)

Figure 3. MSE as function of OMs orders for : **(a)**: ”Deer” binary image, **(b)**: ”Cameraman” grayscaled image, **(c)**: ”Texture” color image .

In the figure 4, it is shown the computing time for reconstruction of previous moments (TMs, KMs, CMs, and HMs) as a function of polynomial orders. The computing time grows exponentially with the order. This is much clearer for CMs and HMs. So far, KMs's computing time is the brief one for binary and grayscale images, followed by TMs.

### *5.2. Classification results*

This section discusses applying the theoretical framework for classification problem. Using Equations 66, we meticulously compute the invariant orthogonal moments of different types noted OMIs for orders up to 3. we could choose more features, but to enhance computational efficiency, we limited our selection to moments' order up to 3.

$$V = \left[OMI_{0,2}(f), OMI_{2,0}(f), OMI_{1,2}(f), OMI_{2,1}(f), OMI_{3,0}(f), OMI_{0,3}(f)\right] \tag{66}$$

The following image databases are used in classification experiments,

- The Handwritten Digits dataset, comprised of 1000 artificial grayscale images of handwritten digits, is a condensed version of the dataset found in [here]. It is a portion of the well-known MNIST data collection, which can be found at [41] and contains $70,000$ in handwritten digits. Every 28-by-28 pixel image has a label attached that indicates the digit it represents, ranging from $0$ to $9$. But in addition, the image has been translated a specific distance and rotated at a specific degree. For each category, there are 100 photographs in the datastore. For every category, there are 70 samples in the training set. The exam makes use of the remaining pictures. Handwritten digits that are part of the database are displayed in Figure 5.

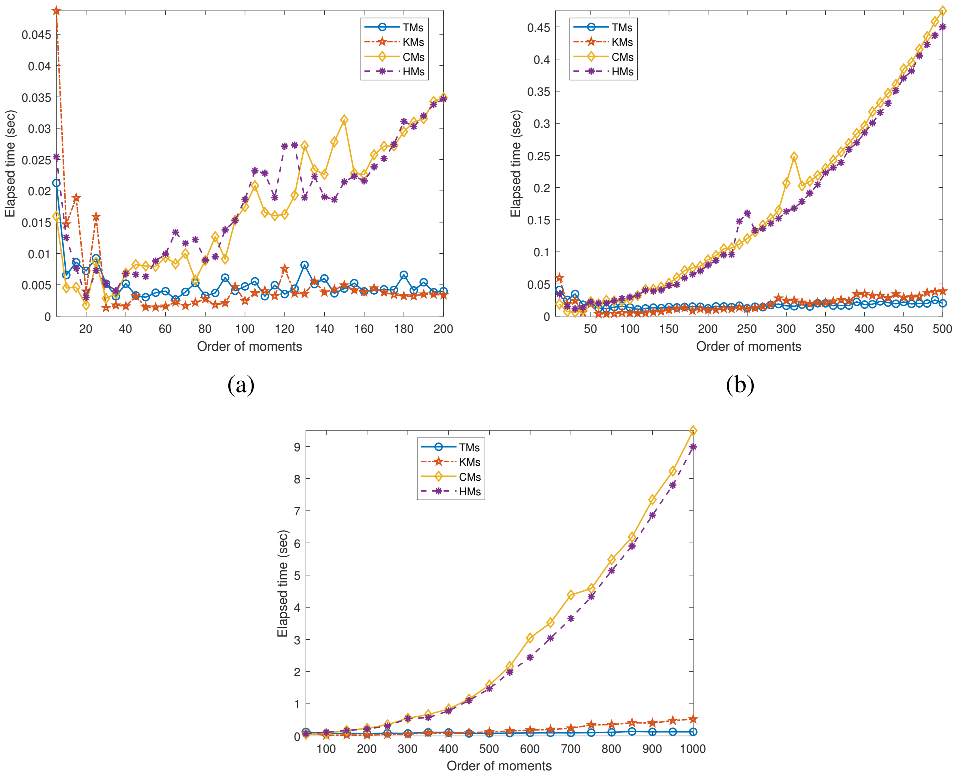

(a) (b)

(c)

Figure 4. Computing Time of discrete orthogonal moments OMs for : **(a)**: Binary image, **(b)**: Garyscale image and **(c)**: Color image as a function of OMs orders.

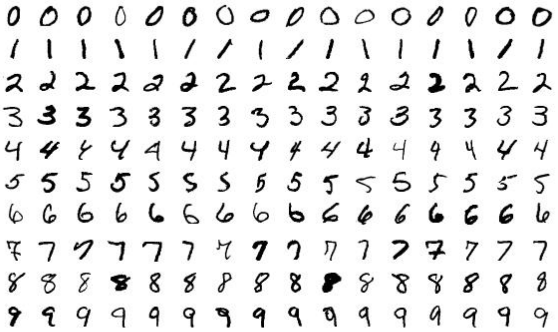

Figure 5. The samples of MNSIT dataset before the preprocessing.

- The second image database located in [42], which is the Columbia Object Image Library $COIL-20$ database, which has 1440 $128 \times 128$ images spread out as 72 images for each item. Nonetheless, the classification model is trained using 45 images from each item category, while additional images are used for testing. The photographs of the objects considered in this database are displayed in Figure 6.

Figure 6. Object considered in COIL-20 database.

- The third database is the Columbia Object Image Library (COIL-100) database, available in [43]. With total number of images equal 7200, categorized as 72 images for each object; however, all the images in this database are in color type, and images in this database have a size of $128 \times I28$. For training of classification models 50 images per category are used, and the rest for test. Figure 7 illustrate the images of objects considered in this database.

Figure 7. Object considered in COIL-100 database.

We apply the following classification criteria to assess the performance of the proposed invariants with respect to recognition accuracy [44, 45].

$$Accuracy = \frac{Number\ of\ correctly\ classified\ images}{Number\ of\ images\ used\ in\ the\ test} \times 100\% \tag{67}$$

Machine learning models provide the basis of the classification methods. Among them are Support Vector Machine (SVM) [46] and k-nearest neighbors (k-NN) [47].

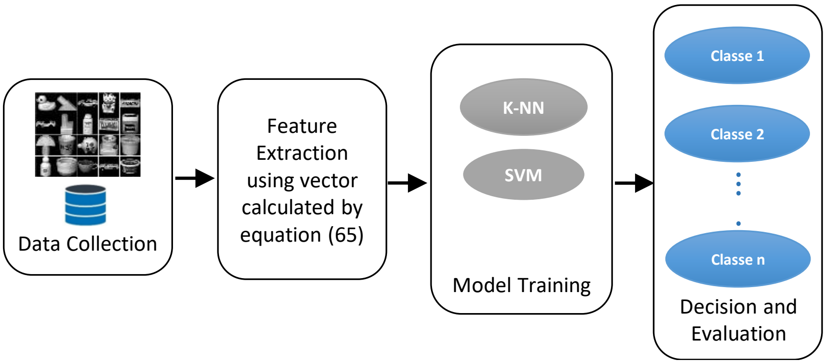

Figure 8. Architecture of classification model using OMIs.

We integrate these models because they are popular choices for classification tasks, including those involving features obtained from orthogonal moments, due to the following considerations:

- Feature Representation: Orthogonal moments are often used in image analysis and pattern recognition because they can represent shapes and patterns effectively. The choice of SVM or k-NN can be influenced by how well these features capture the distinguishing characteristics of different classes.
- Performance Evaluation: The effectiveness of SVM or k-NN with orthogonal moment features can depend on the specific application, dataset, and feature representation. Its often useful to experiment with multiple classifiers and evaluate their performance using metrics such as accuracy, precision.

However, These models have the following attributes:

The comparison's k-NN model has a fine configuration, with the number of nearest neighbors fixed to one. The distance measure used is Euclidean distance. Since the distance weights are set to equal, it may be assumed that each neighbor has an equal influence on the classification outcome. Enabling data standardization guarantees consistent feature scaling, which enhances model performance and makes correct distance calculations easier.

As well as, to ensure flexibility in response to the intrinsic structure of the data, the support vector machine (SVM) model used in this comparison makes use of a quadratic kernel function with an automated kernel scale. By building classifiers for every pair of classes and combining their results, the model effectively handles multiple classes using a one-vs-one multiclass approach. The characteristics are rescaled to have a zero mean and a one standard deviation when data standardization is enabled. The figure 8 illustrates the structure of the classification model.

In order to compare between the studied invariant moments, we take into consideration the elapsed time for reconstruction of the feature vector in (66). Table **??** demonstrates the elapsed time for extracting the features by computing the vector V for all the images in the dataset. This time is computed for each of the studied invariant moments (TMIs, KMIs, CMIs, and HMIs) applied to the feature extraction from the three datasets used. The results are shown in table 5. We note that elapsed time is proportional to the size of database implemented (number of images) and size of the image (dimensions). Where the computational time is increasing with the number and size of images. Nevertheless, CMIs give the best elapsed time over all the other methods. However, the computation is implemented on a personal computer equipped with an Intel Core i5 CPU (2.4 GHz–2.5 GHz) and 8 GB of RAM. However, it is possible to enhance the computational time by parallelization of tasks or using of image block representation (IBR) [48].

The results in Table 6 show that the validation accuracy of both K-Nearest Neighbors (K-NN) and Support Vector Machine (SVM) models varies across moment types and datasets, with SVM generally achieving higher accuracy than K-NN. For the MNIST and COIL-20 databases, CMIs and HMIs provide the best performance for both models, particularly with SVM, indicating that these moment types capture features well for these datasets. In the more complex COIL-100 database, accuracy decreases overall, especially for K-NN with TMIs and RMIs,

Table 5. CPU Elapsed time of TMIs, KMIs, CMIs and HMIs for: part of MNIST, COIL-20, and COIL-100 dataset.

| Database | Elapsed time in seconds (s) | | | |
|---|---|---|---|---|
| | TMIs | KMIs | CMIs | HMIs |
| Part of MNIST dataset (1000 images of size $28 \times 28$) | 1111.080158 | 342.0464 | 4.379137 | 5337.920088 |
| COIL-20 dataset (1440 images of size $128 \times 128$) | 1660.300723 | 363.8819 | 25.525063 | 7602.949929 |
| COIL-100 dataset (7200 images of size $128 \times 128$) | 8108.490066 | 1229.257177 | 121.644441 | 39404.108683 |

Table 6. The validation accuracy of used machine learning classification models using the compared moments, applied to three different databases.

| Database | The trained model | Validation accuracy in % | | | |
|---|---|---|---|---|---|
| | | TMIs | KMIs | CMIs | HMIs |
| The set of MNIST Database | K-Nearest Neighbors (K-NN) | 89.6% | 98.9% | 97.7% | 96.6% |
| | Support Vector Machine (SVM) | 93.1% | 98.7% | 97.3% | 96.7% |
| The COIL-20 Database | K-Nearest Neighbors (K-NN) | 70.4% | 88.3% | 93.6% | 92.4% |
| | Support Vector Machine (SVM) | 78.2% | 90.1% | 93.6% | 91.8% |
| The COIL-100 Database | K-Nearest Neighbors (K-NN) | 45.9% | 78.3% | 89.4% | 89.2% |
| | Support Vector Machine (SVM) | 52.1% | 78.2% | 88.2% | 86.8% |

but CMIs and HMIs still yield relatively high accuracy, especially for SVM. This suggests that CMIs and HMIs are the most effective moment types for image classification tasks across different datasets, with SVM performing consistently well.

Table 7. Classification accuracy of the K-NN and SVM models using TMIs, KMIs, and CMIs moments for the of MNIST, COIL-20 and COIL-100 databases in the absence and presence of salt and pepper noise.

| Database | Classification model | Invariant moments | Free-noise | Salt & Pepper noise | | |
|---|---|---|---|---|---|---|
| | | | | 2% | 3% | 4% |
| The set of MNIST Database | KNN | TMIs | 87.0% | 52.7% | 54.7% | 47.7% |
| | | KMIs | 96.3% | 43.7% | 36.7% | 32.0% |
| | | CMIs | 97.3% | 39.3% | 30.3% | 30.0% |
| | | HMIs | 97.0% | 39.3% | 34.7% | 36.0% |
| | SVM | TMIs | 90.3% | 58.0% | 56.3% | 51.0% |
| | | KMIs | 96.3% | 46.7% | 37.0% | 44.3% |
| | | CMIs | 98.7% | 44.3% | 39.7% | 38.3% |
| | | HMIs | 97.0% | 51.7% | 42.0% | 39.3% |
| COIL-20 Database | KNN | TMIs | 69.8% | 84.8% | 81.1% | 75.9% |
| | | KMIs | 86.9% | 87.4% | 86.1% | 87.6% |
| | | CMIs | 97.2% | 94.1% | 93.3% | 93. % |
| | | HMIs | 100.0% | 94.1% | 94.6% | 76.9% |
| | SVM | TMIs | 78.9% | 88.3% | 81.1% | 79.8% |
| | | KMIs | 90.4% | 89.1% | 90.6% | 88.1% |
| | | CMIs | 94.4% | 92.4% | 91.5% | 93.5 % |
| | | HMIs | 97.1% | 90.7% | 93.5% | 75.4% |
| COIL-100 Database | KNN | TMIs | 48.4% | - | - | - |
| | | KMIs | 80.2% | 78.4% | 78.0% | 76.6% |
| | | CMIs | 91.9% | 88.5% | 86.8% | 84.8% |
| | | HMIs | 68.3% | 62.7% | 55.1% | 47.2% |
| | SVM | TMIs | 52.9% | - | - | - |
| | | KMIs | 79.2% | 76.5% | 76.2% | 75.5% |
| | | CMIs | 90.4% | 86.4% | 85.3% | 84.2% |
| | | HMIs | 68.4% | 53.2% | 43.1% | 35.8% |

The table 7 presents classification accuracy results for K-NN and Support SVM models using four types of invariant moments: TMIs, KMIs, CMIs and HMIs. The results are shown for three datasets, part of MNIST, COIL-100, and COIL-20, under conditions with and without salt and pepper noise.
In summary, CMIs provide the highest classification accuracy and resilience to noise across both MNIST and COIL-20 datasets, with SVM models generally outperforming K-NN models. KMIs offer moderate performance, better than TMIs but lower than CMIs and HMIs, and also demonstrate decent resilience to noise. TMIs have the lowest accuracy, particularly noticeable in the COIL-100 dataset, and show significant performance degradation under noisy conditions. Overall, CMIs are the most effective invariant moments for classification tasks, followed by HMIs, and then KMIs, with TMIs being the least effective, especially in the presence of noise.

From the results presented earlier, we can conclude that the effectiveness of invariant orthogonal moments in terms of classification accuracy is significantly enhanced when combined with machine learning algorithms. This improvement is notable when compared to other recent studies that rely on traditional methods focusing solely on similarity and distance metrics between features, such as in [49]. However, the method proposed in [49] is based on constructing invariants using geometric techniques, which can be computationally intensive. Furthermore, this approach may face limitations when dealing with non-rigid deformations beyond the three basic geometric transformations, where deep learning methods could serve as more flexible and robust alternatives.

## 6. Conclusion

In this study, we have demonstrated the efficacy of and performance of orthogonal moments for image reconstruction, as well as, the robustness of their invariants in image classification and object recognition tasks. By introducing orthogonal moments derived from Tchebichef, Krawtchouk, Charlier, and Hahn polynomials, we explained their computational methods and utilized them to construct feature vectors tailored for each image. These feature vectors were then employed in classification tasks using popular machine learning algorithms, including K-Nearest Neighbors (K-NN) and Support Vector Machine (SVM), to improve classification performance. Our results highlight the robustness of invariant moments in capturing discriminative image features, even in challenging conditions with salt-and-pepper noise, reinforcing their value for reliable recognition and classification in noisy environments. Furthermore, these orthogonal moments hold promising potential for diverse applications, such as medical imaging and biometric identification, where precise and resilient feature extraction is critical.

## REFERENCES

1. W. A. Jassim, P. Raveendran, and R. Mukundan, “New orthogonal polynomials for speech signal and image processing,” *IET Signal Processing*, vol. 6, no. 8, pp. 713–723, 2012.
2. J. Flusser, B. Zitova, and T. Suk, *Moments and moment invariants in pattern recognition*. John Wiley & Sons, 2009.
3. M.-K. Hu, “Visual pattern recognition by moment invariants,” *IRE transactions on information theory*, vol. 8, no. 2, pp. 179–187, 1962.
4. M. R. Teague, “Image analysis via the general theory of moments,” *Josa*, vol. 70, no. 8, pp. 920–930, 1980.
5. P.-T. Yap, R. Paramesran, and S.-H. Ong, “Image analysis by krawtchouk moments,” *IEEE Transactions on image processing*, vol. 12, no. 11, pp. 1367–1377, 2003.
6. L. Kotoulas and I. Andreadis, “Fast computation of chebyshev moments,” *IEEE transactions on circuits and systems for video technology*, vol. 16, no. 7, pp. 884–888, 2006.
7. A. Bourzik, B. Bouikhalene, J. El-Mekkaoui, and A. Hjouji, “A comparative study and performance evaluation of discrete tchebichef moments for image analysis,” in *Proceedings of the 6th International Conference on Networking, Intelligent Systems & Security*, 2023, pp. 1–7.
8. A. M. Abdul-Hadi, S. H. Abdulhussain, and B. M. Mahmmod, “On the computational aspects of charlier polynomials,” *Cogent Engineering*, vol. 7, no. 1, p. 1763553, 2020.
9. A. Bourzik, B. Bouikhalene, J. El-Mekkaoui, and A. Hjouji, “Accurate image reconstruction by separable krawtchouk-charlier moments with automatic parameter selection using artificial bee colony optimization,” *Multimedia Tools and Applications*, pp. 1–22, 2024.
10. A. Bourzik, B. Bouikhalene, J. El−Mekkaoui, and A. Hjouji, “Advanced optimization of discrete orthogonal hahn moments for precision image reconstruction via the firefly algorithm,” in *2024 3rd International Conference on Embedded Systems and Artificial Intelligence (ESAI)*. IEEE, 2024, pp. 1–9.
11. P.-T. Yap, R. Paramesran, and S.-H. Ong, “Image analysis using hahn moments,” *IEEE transactions on pattern analysis and machine intelligence*, vol. 29, no. 11, pp. 2057–2062, 2007.

12. K. M. Hosny, "Image representation using accurate orthogonal gegenbauer moments," *Pattern Recognition Letters*, vol. 32, no. 6, pp. 795–804, 2011.
13. A. Hjouji, B. Bouikhalene, J. EL-Mekkaoui, and H. Qjidaa, "New set of adapted gegenbauer–chebyshev invariant moments for image recognition and classification," *The Journal of Supercomputing*, vol. 77, pp. 5637–5667, 2021.
14. M. El Mallahi, A. Zouhri, J. El-Mekkaoui, and H. Qjidaa, "Radial meixner moments for rotational invariant pattern recognition," in *2017 Intelligent Systems and Computer Vision (ISCV)*. IEEE, 2017, pp. 1–6.
15. C.-W. Chong, P. Raveendran, and R. Mukundan, "Translation and scale invariants of legendre moments," *Pattern recognition*, vol. 37, no. 1, pp. 119–129, 2004.
16. A. Khotanzad and Y. H. Hong, "Invariant image recognition by zernike moments," *IEEE Transactions on pattern analysis and machine intelligence*, vol. 12, no. 5, pp. 489–497, 1990.
17. P.-T. Yap and R. Paramesran, "Jacobi moments as image features," in *2004 IEEE Region 10 Conference TENCON 2004.* IEEE, 2004, pp. 594–597.
18. A. Hjouji, R. Chakid, J. El-Mekkaoui, and H. Qjidaa, "Adapted jacobi orthogonal invariant moments for image representation and recognition," *Circuits, Systems, and Signal Processing*, vol. 40, pp. 2855–2882, 2021.
19. H. Zhu, H. Shu, J. Liang, L. Luo, and J.-L. Coatrieux, "Image analysis by discrete orthogonal racah moments," *Signal Processing*, vol. 87, no. 4, pp. 687–708, 2007.
20. H. Zhu, H. Shu, J. Zhou, L. Luo, and J.-L. Coatrieux, "Image analysis by discrete orthogonal dual hahn moments," *Pattern Recognition Letters*, vol. 28, no. 13, pp. 1688–1704, 2007.
21. A. M. S. Rahma and N. B. Abd, "Detection of a moving car based on invariant moments." *J. Comput. Sci.*, vol. 14, no. 3, pp. 310–316, 2018.
22. J.-L. Coatrieux, "Moment-based approaches in imaging part 2: invariance [a look at...]," *IEEE Engineering in Medicine and Biology Magazine*, vol. 27, no. 1, pp. 81–83, 2008.
23. I. Naouadir, J. El Mekkaoui, A. Hjouji, O. El Ogri, and M. Benslimane, "Tumor detection in mri scans using low order krawtchouk moments," in *2024 Sixth International Conference on Intelligent Computing in Data Sciences (ICDS)*. IEEE, 2024, pp. 1–6.
24. M. T. Ghazal and K. Abdullah, "Face recognition based on curvelets, invariant moments features and svm," *TELKOMNIKA (Telecommunication Computing Electronics and Control)*, vol. 18, no. 2, pp. 733–739, 2020.
25. I. Naouadir, O. El Ogri, J. El Mekkaoui, M. Benslimane, and A. Hjouji, "Celestial object detection in astronomical images using mse and jacobi moments," *Statistics, Optimization & Information Computing*, vol. 12, no. 3, pp. 660–671, 2024.
26. A. Bourzik, B. Bouikhalene, J. El-Mekkaoui, and A. Hjouji, "Invariant tchebichef and krawtchouk moments for shape recognition: A performance evaluation study," in *Proceedings of the 7th International Conference on Networking, Intelligent Systems and Security*, 2024, pp. 1–8.
27. G. Boros and V. Moll, *Irresistible integrals: symbolics, analysis and experiments in the evaluation of integrals*. Cambridge University Press, 2004.
28. R. Mukundan, S. Ong, and P. A. Lee, "Image analysis by tchebichef moments," *IEEE Transactions on image Processing*, vol. 10, no. 9, pp. 1357–1364, 2001.
29. B. H. S. Asli and J. Flusser, "Fast computation of krawtchouk moments," *Information Sciences*, vol. 288, pp. 73–86, 2014.
30. H. Zhu, M. Liu, H. Shu, H. Zhang, and L. Luo, "General form for obtaining discrete orthogonal moments," *IET image processing*, vol. 4, no. 5, pp. 335–352, 2010.
31. M. Sayyouri, A. Hmimid, and H. Qjidaa, "A fast computation of charlier moments for binary and gray-scale images," in *2012 colloquium in information science and technology*. IEEE, 2012, pp. 101–105.
32. J. Zhou, H. Shu, H. Zhu, C. Toumoulin, and L. Luo, "Image analysis by discrete orthogonal hahn moments," in *International Conference Image Analysis and Recognition*. Springer, 2005, pp. 524–531.
33. C. Singh and J. Singh, "Multi-channel versus quaternion orthogonal rotation invariant moments for color image representation," *Digital Signal Processing*, vol. 78, pp. 376–392, 2018.
34. H. Wu and S. Yan, "Computing invariants of tchebichef moments for shape based image retrieval," *Neurocomputing*, vol. 215, pp. 110–117, 2016.
35. Y. Bian, M. Yang, X. Fan, and Y. Liu, "A fire detection algorithm based on tchebichef moment invariants and pso-svm," *Algorithms*, vol. 11, no. 6, p. 79, 2018.
36. R. Zhi, L. Cao, and G. Cao, "Translation and scale invariants of krawtchouk moments," *Information Processing Letters*, vol. 130, pp. 30–35, 2018.
37. A. Hmimid, M. Sayyouri, and H. Qjidaa, "Image classification using separable invariant moments of charlier-meixner and support vector machine," *Multimedia Tools and Applications*, vol. 77, pp. 23 607–23 631, 2018.
38. V. K. Pandey, J. Singh, and H. Parthasarathy, "Translation and scale invariance of 2d and 3d hahn moments," in *2016 3rd International Conference on Signal Processing and Integrated Networks (SPIN)*. IEEE, 2016, pp. 255–259.
39. Z. Iscan, Z. Dokur, and T. Ölmez, "Tumor detection by using zernike moments on segmented magnetic resonance brain images," *Expert systems with applications*, vol. 37, no. 3, pp. 2540–2549, 2010.
40. B. Cyganek, "Circular road signs recognition with affine moment invariants and the probabilistic neural classifier," in *International Conference on Adaptive and Natural Computing Algorithms*. Springer, 2007, pp. 508–516.
41. "The mnist dataset," http://yann.lecun.com/exdb/mnist/, accessed: (March, 2024).
42. "The coil-20 dataset," http://www.cs.columbia.edu/cave/software/softlib/coil-20.php, accessed: (March, 2024).
43. Coil-100, "The coil-100 dataset," http://www.cs.columbia.edu/CAVE/databases, accessed: (March, 2024).
44. A. Hjouji, M. Jourhmane, J. El-Mekkaoui, H. Qjidaa, and A. El Khalfi, "Image clustering based on hermetian positive definite matrix and radial jacobi moments," in *2018 International Conference on Intelligent Systems and Computer Vision (ISCV)*. IEEE, 2018, pp. 1–6.
45. A. Hjouji, J. El-Mekkaoui, M. Jourhmane, H. Qjidaa, and B. Bouikhalene, "Image retrieval and classication using shifted legendre invariant moments and radial basis functions neural networks," *Procedia computer science*, vol. 148, pp. 154–163, 2019.

46. M. A. Hearst, S. T. Dumais, E. Osuna, J. Platt, and B. Scholkopf, "Support vector machines," *IEEE Intelligent Systems and their applications*, vol. 13, no. 4, pp. 18–28, 1998.
47. L. E. Peterson, "K-nearest neighbor," *Scholarpedia*, vol. 4, no. 2, p. 1883, 2009.
48. G. A. Papakostas, E. G. Karakasis, and D. E. Koulouriotis, "Accurate and speedy computation of image legendre moments for computer vision applications," *Image and Vision Computing*, vol. 28, no. 3, pp. 414–423, 2010.
49. R. Mukundan, "Radial tchebichef invariants for pattern recognition," in *TENCON 2005-2005 IEEE Region 10 Conference*. IEEE, 2005, pp. 1–6.